JACS
JOURNAL OF THE AMERICAN CHEMICAL SOCIETY

Article

pubs.acs.org/JACS

Insights into the Glycyl Radical Enzyme Active Site of Benzylsuccinate Synthase: A Computational Study

Vivek S. Bharadwaj, Anthony M. Dean, and C. Mark Maupin*

Chemical and Biological Engineering Department, Colorado School of Mines, 1500 Illinois Street, Golden, Colorado 80401, United States

Supporting Information

ABSTRACT: The fumarate addition reaction, catalyzed by the enzyme benzylsuccinate synthase (BSS), is considered to be one of the most intriguing and energetically challenging reactions in biology. BSS belongs to the glycyl radical enzyme family and catalyzes the fumarate addition reaction, which enables microorganisms to utilize hydrocarbons as an energy source under anaerobic conditions. Unfortunately, the extreme sensitivity of the glycyl radical to oxygen has hampered the structural and kinetic characterization of BSS, thereby limiting our knowledge on this enzyme. To enhance our molecular-level understanding of BSS, a computational approach involving homology modeling, docking studies, and molecular dynamics (MD) simulations has been used to deduce the structure of BSS's catalytic subunit (BSSα) and illuminate the molecular basis for the fumarate addition reaction. We have identified two conserved and distinct binding pockets at the BSSα active site: a hydrophobic pocket for toluene binding and a polar pocket for fumaric acid binding. Subsequent dynamical and energetic evaluations have identified Glu509, Ser827, Leu390, and Phe384 as active site residues critical for substrate binding. The orientation of substrates at the active site observed in MD simulations is consistent with experimental observations of the *syn* addition of toluene to fumaric acid. It is also found that substrate binding tightens the active site and restricts the conformational flexibility of the thiyl radical, leading to hydrogen transfer distances conducive to the proposed reaction mechanism. The stability of substrates at the active site and the occurrence of feasible radical transfer distances between the thiyl radical, substrates, and the active site glycine indicate a substrate-assisted radical transfer pathway governing fumarate addition.

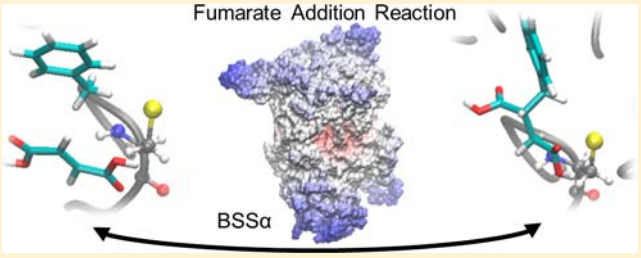

1. INTRODUCTION

Glycyl radical enzymes (GREs) catalyze some of the most remarkable and energetically challenging free radical reactions encountered in biology.[1−3] One of these particularly important reactions is the fumarate addition reaction, which is the first step in the anaerobic metabolism of hydrocarbons.[4,5] The GRE benzylsuccinate synthase (BSS) catalyzes this reaction, thereby enabling sulfate, nitrate, and iron reducing bacterial cultures to thrive on hydrocarbons as their primary carbon source.[6] The growth of these microorganisms on metallic surfaces has a detrimental impact as it facilitates biocorrosion in oil pipelines and storage facilities.[7] Biocorrosion is also a significant problem on naval vessels equipped with seawater-compensated fuel ballast tanks, which must be periodically dry docked for repairs. Recent studies indicate that biofuels are more susceptible to undergo biodegradation than conventional fossil fuels.[8] With a continuing shift toward the widespread use of biofuels, it is believed that the adverse impact of biocorrosion will be exacerbated. Therefore, a fundamental understanding of the fumarate addition reaction is necessary to guide the selection of future fuel components and/or development of inhibitors. Understanding the ability of these microorganisms to metabolize hydrocarbons also has potential benefits in bioremediation of oil-contaminated soil and aqueous environments[5] since aromatic hydrocarbons like benzene, toluene, ethyl-benzene, and xylenes are known to be toxic, hazardous pollutants.[9]

The intriguing free radical catalysis in BSS has been the subject of various studies over the past decade.[2,10−15] Studies on the subunit structure of BSS suggest that it exists as a heterohexamer ($\alpha_2\beta_2\gamma_2$) with the catalytic dyad (Cys492 and Gly828) located in the α subunit.[10] The catalytic dyad is known to be conserved among all known GREs with the glycine believed to be responsible for harboring the radical and the cysteine residue responsible for mediating catalysis.[2] Krieger et al. conducted electron paramagnetic resonance (EPR) studies establishing the glycyl-based radical in BSS and proposed the catalytic mechanism shown in Scheme 1.[11] The first step in the suggested mechanism involves the H-abstraction from the toluene substrate by the cysteine radical (Cys492•). The resulting benzyl radical then adds to fumaric acid, forming the succinyl radical intermediate, which then abstracts the hydrogen from Cys492, to regenerate the radical for subsequent catalysis.

Received: May 14, 2013
Published: July 18, 2013

dx.doi.org/10.1021/ja404842r | J. Am. Chem. Soc. 2013, 135, 12279−12288

Scheme 1. Steps Involved in the Proposed Catalytic Mechanism for BSS Mediated by the Cysteine Radical (Cys492•)[a]

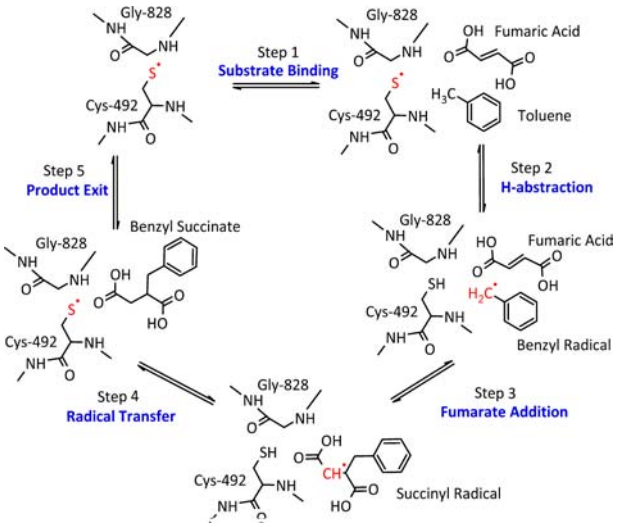

[a]The location of the radical at each step is denoted by the symbol '•' and is shown in red.

Upon exposure to oxygen, GREs are inactivated due to cleavage at the radical site[16] making their detailed structural and kinetic characterization challenging. In the case of BSS, this has precluded its structural characterization[10] and limited the current understanding of the mechanism at the molecular level and the energetic and steric effects governing substrate and product binding in BSS. Although the feasibility of the proposed reaction mechanism has been demonstrated theoretically with a highly reduced molecular model,[17] the role of the enzyme structure in facilitating this remarkable reaction is currently unknown.

With the advent of computational structure prediction techniques such as homology modeling, it is now possible to predict the 3D structure of a protein based on its amino acid sequence and structural information from genetically and/or functionally related proteins. Homology modeled structures have been successfully used in gaining significant insights into enzymatic mechanisms and substrate binding energetics.[18−24] In this study, homology modeling has been used to provide the structural basis from which the BSS active site topology has been elucidated using docking techniques and guided by existing experimental insights.[12,25] Specific enzyme−substrate interactions that facilitate substrate and product binding in BSS have been identified using molecular dynamics simulations (MD) and subsequent geometric and energetic analyses. The parameterization of the cysteine radical coupled with umbrella sampling techniques have enabled the evaluation of the impact of substrate and product binding on the dynamics of the active site as well the conformational flexibility of the thiyl radical. The results of this study provide a structural basis to not only interpret available biochemical data but also gain molecular-level insights into BSS's radical catalytic mechanism. This sound structural basis will be critical in bridging the gap between the lack of experimental structural data on BSS and the pressing need to understand the molecular basis governing anaerobic biodegradation of hydrocarbons, thereby addressing issues in the larger context of biocorrosion and bioremediation.

2. METHODS

2.1. Homology Modeling. The amino acid sequence for the catalytic subunit of BSS from the denitrifying bacterial strain *Thauera Sp.* DNT-1 was obtained from the NCBI database (accession no. BAC05501).[26] The *Thauera Sp.* DNT-1 bacterial strain was chosen since it offers a complete available sequence of the BSS operon and is hence amenable to experimental investigations. The catalytic subunit of BSS (BSSα) has a total of 864 amino acids with the putative radical sites located on Cys492 and Gly828. The Basic Local Alignment Search Tool (BLAST)[27] was used to search the protein databank (PDB) to find suitable templates for the homology model. Structures with the highest sequence identity were all GREs: glycerol dehydratase (GDH) (PDB ID: 1R8W),[28] a GRE from *Arcaheoglobus fulgidus* (PDB ID: 2F3O),[29] and pyruvate formate lyase (PFL) (PDB ID: 2PFL).[30] For this study, the available crystal structures for GREs (GDH, PFL, and a GRE from *Arcaheoglobus fulgidus*) were all chosen as templates. Modeler v9.10[31] was used with multiple sequence alignment to maximize the use of available structural information from the templates for preparing the homology model of BSSα. The multiple sequence alignment, performed using Salign,[32] of the BSSα sequence with the templates indicated conserved homologous catalytic regions (Supporting Information Figure 1).

A total of 100 homology models were created, and the model with the highest GA341[33] score (i.e., 1) and the lowest discrete optimization potential energy (DOPE)[34] was chosen for subsequent refinements. The selected structure was minimized for 100 steps using the conjugate gradient algorithm in the UCSF Chimera package.[35] Atom−atom clashes in this structure were detected, and further minimizations were carried out for these structural regions. The verify3D[36] and PROCHECK[37] packages were used to assess the quality of the final refined homology modeled structure.

2.2. Docking Calculations. The AutoDock suite of programs has been successfully used in the past for detection of enzyme active sites and substrate binding modes.[38−40] In this study, Autodock v4.2 and AutoDockTools (ADT v1.5.6)[41] were used for two purposes, namely, active site refinement by side chain optimization using a manual induced-fit product docking approach and to generate initial configurations for substrate-bound MD simulations based on the refined active site topology.

The standard protocol of merging nonpolar hydrogens, assigning Gasteiger charges and Autodock atom types, was followed to prepare ligand and receptor input files. Prior to docking, torsions in the ligands (benzylsuccinate, toluene, and fumaric acid) were specified, and residues at the active site were kept flexible (induced fit approach). The active site residues Val708, Leu491, and Leu390 were kept flexible based on initial docking studies that indicated steric clashes with substrate and product molecules thereby restricting access to the active site cysteine (Cys492). A grid box (18 Å × 18 Å × 18 Å) was centered on Cys492 to encompass the active site cavity with the default grid spacing of 0.375 Å. The docking calculations utilized the standard AutoDock force field and the Lamarckian Genetic Algorithm (LGA) search for the lowest energy docked ligand conformers. Each docking experiment consisted of 100 independent LGA runs with the maximum number of energy evaluations for each LGA run set at 2 500 000 with the generations set to a maximum of 27 000. The resulting docking poses were analyzed based on their AutoDock binding energies as well as their spatial orientation to ensure feasibility of the fumarate addition mechanism.

To evaluate the utility of the outlined homology modeling coupled with the docking approach, the methodology was tested on the structurally characterized GRE system of GDH. The results of the validation exercise indicate that this approach can indeed reproduce substrate binding at the active site of GDH. The procedure and detailed results can be found in section 1 of the Supporting Information.

2.3. Molecular Dynamics (MD) Simulations. The fumarate addition reaction is known to be catalyzed by the cysteine radical (Scheme 1).[11] Hence, for representative MD simulations of the substrates and product at the active site, the cysteine radical was

parameterized. A new amino acid residue type (CYR) including a new atom type for sulfur (SV) was defined in the ff99SB[42] force field using antechamber and the restricted electrostatic potential (RESP) derived charges (Supporting Information Section 2).

All MD simulations were conducted with the Amber12 and AmberTools12 software packages.[43] For the protein−substrate complexes, the ff99SB[42] force field was used for the protein and the Generalized Amber Force Field (GAFF)[44] force field for ligand/s. The following seven systems were created: (i) BSSα nonradical form, (ii) BSSα radical form (Cys492•), (iii) BSSα radical (Cys492•) with fumaric acid, (iv) BSSα radical (Cys492•) with toluene, (v) BSSα radical (Cys492•) with toluene and fumaric acid, (vi) BSSα radical (Cys492•) with *R*-benzylsuccinate, and (vii) BSSα radical (Cys492•) with *S*-benzylsuccinate. Although experimentally it is known that fumarate is the substrate for BSS, the active site of BSS is largely hydrophobic in nature and would not provide an environment conducive for charge separation. For this reason, fumaric acid instead of fumarate was used to model the catalytic mechanism for BSS and has hence also been used as the substrate in this study.[17]

The protonation states of the amino acid residues were determined using the H++ online webserver.[45] The systems were created using tleap[43] with explicit water molecules modeled using the TIP3P[46] water model. The resulting system had 31 877 water molecules in a box of dimensions 114 Å × 121 Å × 92 Å (109 233 atoms). The systems were minimized for 2000 steps using the conjugate gradient algorithm. The minimized systems were then equilibrated for 1 ns in the isothermal isobaric (NPT) ensemble. A 20 kcal/mol restraint was employed on the ligand(s) and the Cys492/Cys492• and Gly828 α-carbon atoms during the minimization and equilibration stages. The post equilibration simulations consisted of 40 ns unrestrained production MD runs in the canonical (NVT) ensemble. All simulations were conducted with the hydrogen atoms restrained using the SHAKE algorithm[47] and a time step of 2 fs. Analysis of the trajectories was done using VMD[48] and ptraj,[43] and standard deviations were calculated for values reported based on these simulations and were obtained by performing block averaging on the 40 ns trajectory. The block averaging involved splitting the 40 ns trajectory into four blocks of 10 ns each and analyzing each block.

2.4. Binding Energy Calculations. The molecular mechanics/generalized born solvent accessibility (MM/GBSA) implementation in Amber12 was utilized for the calculation of relative binding energies.[49,50] The energies were averaged over 1000 frames taken at intervals of 20 ps. In the MM/GBSA method, the binding energies are calculated as the sum of molecular mechanical and solvation energies as described by eq 1

$$\Delta G_{\text{bind}} = \Delta E_{\text{MM}} + \Delta G_{\text{solv}} - T\Delta S \quad (1)$$

where ΔE_{MM} is the molecular mechanical energy; ΔG_{solv} is the solvation energy which together make up the enthalpic contribution; T is the temperature in Kelvin; and ΔS is entropy.

ΔE_{MM} is calculated using a molecular mechanical force field according to eq 2.

$$\Delta E_{\text{MM}} = \Delta E_{\text{internal}} + \Delta E_{\text{electrostatic}} + \Delta E_{\text{vdw}} \quad (2)$$

where $\Delta E_{\text{internal}}$ is the bond, angle, and dihedral energy contribution; $\Delta E_{\text{electrostatic}}$ is the electrostatic energy contribution; and ΔE_{vdw} is the van der Waals energy contribution. The solvation energy is calculated according to eq 3.

$$\Delta G_{\text{solv}} = \Delta G_{\text{GB}} + \Delta G_{\text{SA}} \quad (3)$$

where ΔG_{GB} is the electrostatic solvation energy and ΔG_{SA} is the nonpolar solvation component. The electrostatic contribution is calculated using the generalized born (GB) model, and the nonpolar component is estimated by solvent-accessible surface area. The physiological salt concentration of 0.15 M was employed for these calculations.

The entropic contributions to free energy were not considered in this study due to their high computational cost, low prediction accuracies, and the lack of experimental data on the binding/inhibition constants for BSS.[51,52] For this study, the calculated binding energies only serve as an additional validation of the predicted active site topology by demonstrating the energetic feasibility of substrate binding and to identify critical amino acids that facilitate binding.

Energy decomposition and computational alanine scanning experiments have been successfully applied for elucidating important enzyme−substrate interactions in various biological systems.[53−58] This approach was used here employing the sander implementation in Amber12. Specific enzyme−substrate interactions that stabilize the ligands (fumaric acid, toluene, and benzylsuccinate) were identified by decomposing the MM/GBSA energies among the active site residues. The effect of these identified residues on substrate binding energies ($\Delta\Delta G_{\text{residue}} = \Delta G_{\text{alanine mutant}} - \Delta G_{\text{wild type}}$) was then evaluated using MM/GBSA calculations on alanine mutants. In this case, the entropic contributions can be justifiably neglected since they essentially cancel out in the $\Delta\Delta G$ calculations and hence provide a more accurate insight into the free-energy contribution of a particular residue to substrate binding. The alanine scanning experiments were performed on the 40 ns trajectory of BSSα with both substrates (toluene and fumaric acid) bound.

2.5. Potential of Mean Force (PMF) Calculations. The proposed reaction mechanism for BSS assumes that the active site cysteine mediates the reaction as in other GRE systems. This active site cysteine is located between the substrates and the buried and substrate-inaccessible active site glycine (that harbors the radical), thereby possibly acting as a shuttle for radical transfer. The presence of the radical on the sulfur atom of cysteine enables its access to a larger conformational space, thus impacting radical transfer distances involved in the reaction mechanism. The rotation about the dihedral angle (N−C_α−C_β−S) of cysteine describes the thiyl radical's conformational flexibility and was hence chosen as the reaction coordinate for the PMF calculations. The biased umbrella sampling technique along with the unbiasing weighted histogram analysis method (WHAM) were utilized for the construction of the PMFs.[59−61] Comparison of the PMFs for dihedral rotation in the unbound enzyme and in the presence of the substrates and product allowed for the evaluation of the impact of substrate and product binding on the flexibility of the thiyl radical. The restraining potential used was of the form shown in eq 4.

$$U_n^{\text{umbrella sampling}}(\xi_{\text{dihedral}}) = \frac{k_n}{2}(\xi_{\text{dihedral}} - \xi_0^n)^2 \quad (4)$$

where $U_n^{\text{umbrella sampling}}$ is the restraining potential; k_n denotes the force constant for the restraining potential; ξ_0 denotes the equilibrium value of the dihedral angle for each window; and ξ_{dihedral} denotes the instantaneous value of the dihedral angle. The umbrella sampling simulations were spawned across 21 windows (spaced every 10°) in the range of −100° to 100° with a restraining potential force constant of 40 kcal/mol·rad^2 on the dihedral angle. Each window was equilibrated for 250 ps followed by a production run varying from 2 to 4 ns depending on the convergence of the PMF in each window. The convergence of the PMFs was verified by performing the bootstrap analysis incorporated in the WHAM code which revealed errors ≤0.1 kcal/mol.[61]

3. RESULTS AND DISCUSSION

3.1. BSSα Homology Model. A molecular-level understanding of the catalytic mechanism in BSS has thus far been elusive due to the unavailability of an experimentally determined structure for BSS. However, the remarkable structural homology demonstrated by the enzymes of the GRE family and modern homology modeling techniques that exploit these structural similarities provide a route to elucidate the structure of BSS. The results of the BLAST search revealed that the amino acid sequence similarity between BSSα and the GRE family is between 26% and 30% (Supporting Information Table 3). The multiple-sequence alignment (Supporting Information Figure 1) of BSSα with the templates indicates

Table 1. Matrix Depicting Sequence and Structural Similarity Amongst GREs[a]

	BSSα	GDH	GRE (*Arch* Fulg.)	PFL	HPA-D
BSSα	-	30%	27%	26%	24%
GDH	0.7 Å	-	36%	28%	29%
GRE (*Arch. Fulg*)	1.1 Å	1.1 Å	-	23%	27%
PFL	1.1 Å	1.1 Å	1.2 Å	-	22%
HPA-D	1.2 Å	1.2 Å	1.3 Å	1.3 Å	-

[a]The top right half of the matrix denotes percentage sequence identity, and the bottom left half denotes RMSD values upon superposition of the 3-D structures. Abbreviations used for the glycyl radical enzymes: GDH, glycerol dehydratase (PDB ID: 1R8W); GRE (*Arch. fulg.*), a glycyl radical enzyme from *Archaeoglobus fulgidus* (PDB ID: 2F3O); PFL, pyruvate formate lyase (PDB ID: 2PFL); HPA-D, hydroxy phenyl acetate-decarboxylase (PDB ID: 2Y8N).

that although there is low overall primary sequence similarity there is significant conservation in the central and C-terminal regions including the glycl/thiyl dyad. In spite of the fact that GREs share low sequence identities, they have been shown to have highly conserved 3-D structures, which is illustrated by the relatively low root mean squared displacement (RMSD) values of ∼1 Å in homologous regions (Table 1).[2]

A schematic representation of the secondary structure of the BSSα homology model is shown in Figure 1. It is evident that

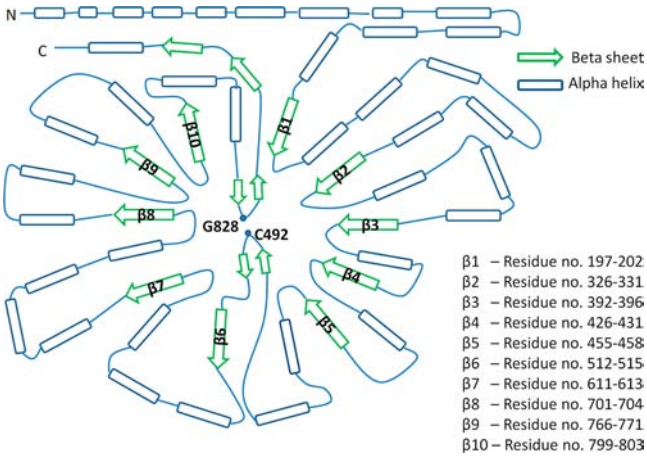

Figure 1. Canonical glycyl radical enzyme structural motif as observed in the homology model of BSSα. The putative radical sites Gly828 and Cys492 are situated at the apex of two loops facing each other and separated by 4.4 Å.

the canonical GRE fold,[62] observed in GRE structures,[28−30] is also conserved in the BSSα homology model. In addition, the BSSα homology model has the putative radical sites Gly828 and Cys492 situated at the core of the enzyme and surrounded by the characteristic 10-stranded α/β barrel.

The homology model was subsequently analyzed using the Verify3D[36] package, which quantifies the compatibility of the tertiary structure to its primary amino acid sequence. The verify3D analysis (Supporting Information Figure 4) indicates good compatibility of the homology model with its amino acid sequence. The Ramachandran plot statistics for the homology model reveal that 97.3% of the residues are present in the core and allowable regions, 2.1% in the generously allowable regions, and only 0.7% of the residues in the disallowed regions, thus indicating good stereochemical quality.

The structure of BSS has been suggested to be similar to that of another GRE, hydroxyphenyl acetate decarboxylase (HPA-D), since both enzymes are multimeric GREs.[10] The recently published crystal structure of HPA-D (PDB ID: 2Y8N) is the first crystal structure of a heteromeric GRE and reveals that HPA-D exists as a heterooctamer.[62] Since the BSSα homology model was made before the HPA-D crystal structure was published, it was not used as a template in this study. However, a structural comparison of the BSSα homology model with HPA-D serves as another test of the structural conservation among GREs. The structural alignment reveals a RMSD of 1.2 Å for the homologous regions, with a sequence identity of 24%. The canonical GRE fold with the 10 stranded α/β barrel and the glycyl/thiyl residues at the apex of two loops is also observed to be conserved between the two structures. The Cα distance for the glycyl/thiyl dyad is found to be 4.5 Å in HPA-D structure as compared to 4.4 Å in the BSSα homology model. The significant structural conservation among GREs in the presence of low primary sequence identity indicates that the homology modeling can indeed be used to provide a platform for elucidating the BSSα's active site topology.

3.2. Elucidation of the Active Site Topology in BSSα.

Although GREs share a conserved structural motif, they catalyze reactions involving different substrates. The absence of fumaric acid and/or toluene as substrates in previously structurally characterized GRE systems necessitated the refinement of the active site topology in the BSSα homology model. The induced fit docking strategy involves docking calculations of the ligand with flexible amino acid residues at the binding site. Since the fumarate addition reaction forms an addition product (benzylsuccinate), an active site topology capable of accommodating the product should, in principle, be able to accommodate the reactants. With this rationale, induced fit docking studies of the benzylsuccinate product were carried out to refine the active site.

It has been experimentally observed from deuterium labeling studies that the very same hydrogen abstracted from toluene is retained in the product benzylsuccinate molecule[25] and that the addition of toluene to fumaric acid is of *syn* nature.[12] These insights suggest that the productive active site topology of BSSα must satisfy the following criteria:

i. Conduct the *syn* addition of toluene to fumaric acid.
ii. Position substrates suitably to facilitate feasible H-transfer reactions for the mechanism while resulting in the formation of a succinyl moiety that contains the hydrogen atom originally abstracted from toluene.
iii. Favorably (energetically) bind both substrates.

Furthermore, the fumarate addition in BSS is experimentally found to be highly stereospecific resulting in predominantly the

R-stereoisomer.[25] The chirality of the methyl carbon of toluene upon addition to fumaric acid dictates the configurational stereochemistry of the resulting benzylsuccinate product which can either be an *R*- or *S*-stereoisomer. The active site elucidation using the induced fit approach was carried out for both stereosiomers, which revealed a similar topology in both cases. Figure 2 depicts the elucidated active site topology with

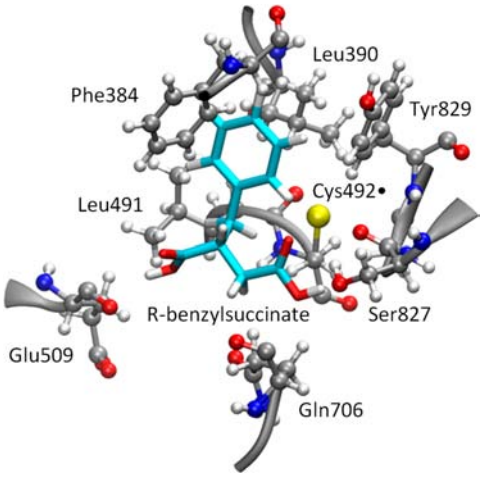

Figure 2. Active site topology and *R*-benzylsuccinate binding pose obtained from results of the induced fit docking calculations. The benzylsuccinate molecule is shown in licorice representation with the carbon atoms colored cyan. The protein backbone and the residues are indicated with ribbon and CPK representations, respectively.

the *R*-benzylsuccinate bound. It is observed that the benzyl ring (toluene portion) of the succinate molecule is surrounded by hydrophobic residues Leu491, Phe384, Leu390, and Tyr829, and the carboxyl regions of the succinate molecule (fumaric acid portion) are close to potential H-bonding interactions with Ser827, Glu509, and Gln706. It is evident that this active site topology offers two distinct binding pockets suited specifically for toluene and fumaric acid binding. This was verified with independent docking studies of toluene and fumaric acid at the active site (Supporting Information Section 3).

The fumarate addition reaction has been observed in various bacterial species that metabolize toluene.[63−66] A multiple sequence alignment, performed using ClustalW,[67] of the amino acid sequence of BSSα from four other species of bacteria (Figure 3) reveals 100% conservation of the hydrophobic and polar amino acid residues that form the putative binding pockets for toluene and fumaric acid at the active site. The conserved nature of these amino acids strongly suggests that these residues are critically important to the binding of toluene and fumaric acid. The two distinct binding pockets create the opportunity for site-specific mutations to probe the importance of these residues and evaluate the impact of substrate binding on the catalysis of BSSα. The role played by these residues is discussed in detail in the next section.

3.3. Enzyme−Substrate Interactions. Typical lifetimes of radical intermediates in enzymatic radical reactions have recently been observed to be around 10 ns.[68] This necessitates the stable accommodation of toluene, fumaric acid, and benzylsuccinate at the BSSα active site over similar time scales, which has been demonstrated here using MD simulations along with the specific enzyme−substrate interactions responsible for substrate/product binding. These interactions were evaluated using geometric criteria, i.e., hydrophobic interaction distances and hydrogen bonding analyses, as well as energetic criteria, i.e., MM/GBSA binding energies and its decomposition among active site residues.

Before conducting MD simulations of the enzyme−substrate complex, the stability of the homology model was verified using two independent long-time (185 and 100 ns) MD simulations in a solvated environment. The resulting MD trajectory indicated a stable active site with a RMSD of 2.5 Å and root mean square fluctuations (RMSFs) < 0.5 Å in both cases (Supporting Information Figures 6 and 7 and Section 4).

Upon evaluating the structural fitness of the BSSα homology model, docking calculations to the equilibrated structure were conducted, and the binding poses obtained from docking calculations were used as starting points for substrate-bound MD simulations. Systems of BSSα with (i) toluene alone, (ii) fumaric acid alone, (iii) toluene and fumaric acid, and (iv) benzylsuccinate at the active site were run for 40 ns after an initial equilibration of 1 ns in the NVT ensemble. The RMSDs of the active site amino acid residues were found to stabilize at ∼2 Å for all systems, in agreement with the long time MD simulations. Specific enzyme−substrate interactions observed for substrates (Section 3.3.1 and 3.3.2) and product (Section 3.3.3) are discussed in detail below.

3.3.1. Toluene Binding. The favorable binding energetics for toluene binding at the active site (Figure 4.a.1 and 4.a.2) are found to be driven by interactions with hydrophobic residues. These interactions were revealed by the MM/GBSA decomposition analysis (Supporting Information Figure 8) as well as the geometric analysis of toluene's interactions at the active site, which were quantified by tracking the separation distances over the course of the MD simulations (Figure 4.a.1 and 4.a.2 and Supporting Information Table 4). The cluster of hydrophobic residues, Phe384, Leu390, Leu491, Tyr829, and Val708 is

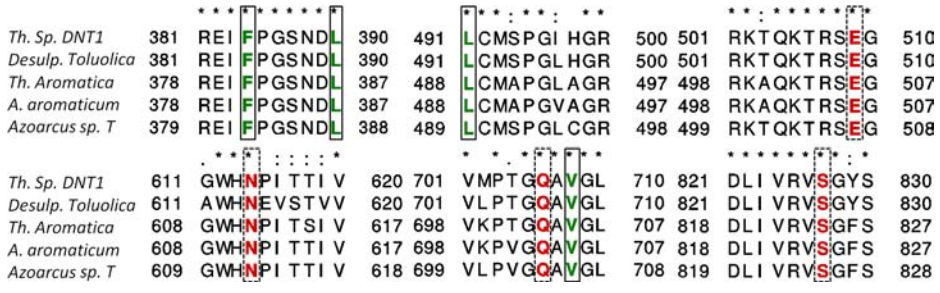

Figure 3. Multiple sequence alignment of the amino acid sequence of BSSα in different bacterial species: *Thauera sp.* DNT 1[26] (used in this study), *Desulphobacula toluolica*,[63] *Thauera aromatica*,[64] *Aromatoleum aromaticum*,[65] and *Azoarcus sp.* T.[66] The hydrophobic (Phe384, Leu390, Leu491, Val708 − continuous boxes) and polar amino acid residues (Glu509, Asn614, Gln706, Ser827 - dashed boxes) are conserved among all species.

dx.doi.org/10.1021/ja404842r | J. Am. Chem. Soc. 2013, 135, 12279−12288

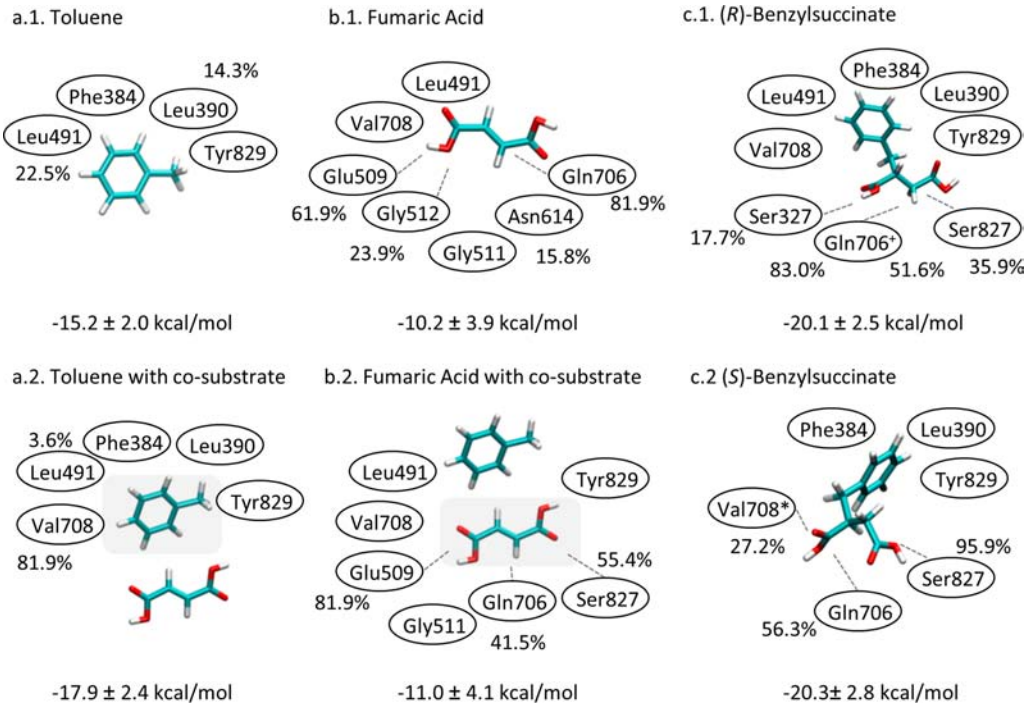

Figure 4. Active site residues identified to aid substrate binding using decomposition analysis. All residues having binding contributions greater than 0.5 kcal/mol are listed, and hydrogen bonding networks are depicted with dashed lines. The geometric analysis has been quantified and denoted as a percentage of the simulation time for which interactions (hydrophobic or hydrogen-bonding) were observed. Also listed are the MM/GBSA binding energies for each system, the negative values indicate favorable binding at the active site. *The hydrogen bonding contributions from Val708 are from the protein backbone nitrogen atom. +Hydrogen bonds formed with two different atoms in Gln706.

found to aid toluene binding. It is to be noted that the residues comprising this hydrophobic pocket are conserved in BSSα found in other bacterial cultures (Figure 3). The presence of fumaric acid is found to increase toluene's interactions with Val708, restricting its mobility and thus increasing the chances for H-transfer to the thiyl radical (discussed in detail in Section 3.5).

In the MD simulations involving toluene, especially in the presence of fumaric acid, two observations stand out. First, the toluene methyl group was found to adopt conformations that enable feasible H-transfer with the sulfur atom of Cys492•. The heavy atom distance in the toluene−CH_3S• H-transfer transition state based on quantum mechanical (QM) studies is 3.01 Å.[17] This is similar to the closest distance of ∼3.25 Å that is consistently observed in our MD simulations, for the corresponding hydrogen transfer distance, i.e., toluene's methyl carbon and Cys492•'s sulfur atom. Second, during the course of the 40 ns simulation involving toluene and fumaric acid, it was observed that the predicted toluene binding pocket consistently facilitates the *syn* addition of toluene to fumaric acid (Figure 5b).

3.3.2. Fumaric Acid Binding. While hydrophobic interactions are found to drive toluene binding, H-bonding networks at the active site are found to be critical for fumaric acid binding. The hydrogen bonds observed during the 40 ns simulation of fumaric acid alone and along with toluene at the active site are denoted and quantified in Figure 4.b.1 and 4.b.2 and Supporting Information Table 5. It is found that the carboxyl groups on fumaric acid act as both donors and acceptors for hydrogen bonds with Ser827, Glu509, and Gln706. The importance of these active site residues in fumaric acid binding is also revealed from the MM/GBSA decomposition analysis (Supporting Information Figure 8) and reaffirmed by their conservation among the other bacterial species demonstrating fumarate addition (Figure 3).

It is known that the presence of substrates at the active site in GREs results in a more compact active site configuration favorable for the catalytic event as observed by tighter van der Waals contacts in the crystal structures.[62] This compacting of the active site is also observed in the BSSα homology model. In the presence of toluene, fumaric acid is stabilized at the active site by hydrogen bonds with Glu509, Ser827, and Gln706 (Figure 5b), whereas in the absence of toluene, fumaric acid interactions are observed to be more prominent with residues on the outer regions of the productive binding pocket (Gly512 and Asn614) as shown in Figure 5c. This is reflected in the H-bonding networks and decomposition energies of fumaric acid, when present alone and with toluene at the active site (Figure 4b and Supporting Information Table 5). Furthermore, in MD simulations where the Glu509 and Ser 827 were beyond H-bonding distance from fumaric acid, it was observed that fumaric acid diffused away from the active site region, indicating the importance of these residues in stabilizing fumaric acid at the active site.

3.3.3. Benzylsuccinate Binding. The ability of BSS to catalyze the reverse reaction has been experimentally demonstrated by the exchange of *p*-cresol with the benzyl portion of benzylsuccinate to form 4-hydroxy-benzylsuccinate.[14] This implies that the product benzylsuccinate molecule must also be stable enough at the active site to undergo the reversible reaction described above. MD simulations of both *R*- and *S*-benzylsuccinate at the active site reveal that the succinate product is indeed stable at the active site. A hydrogen bonding network involving Ser827 and Gln706 residues aids this stability (Figure 4.c.1 and 4.c.2 and Supporting Information Table 6). The decomposition analysis also indicates that benzyl

dx.doi.org/10.1021/ja404842r | J. Am. Chem. Soc. 2013, 135, 12279−12288

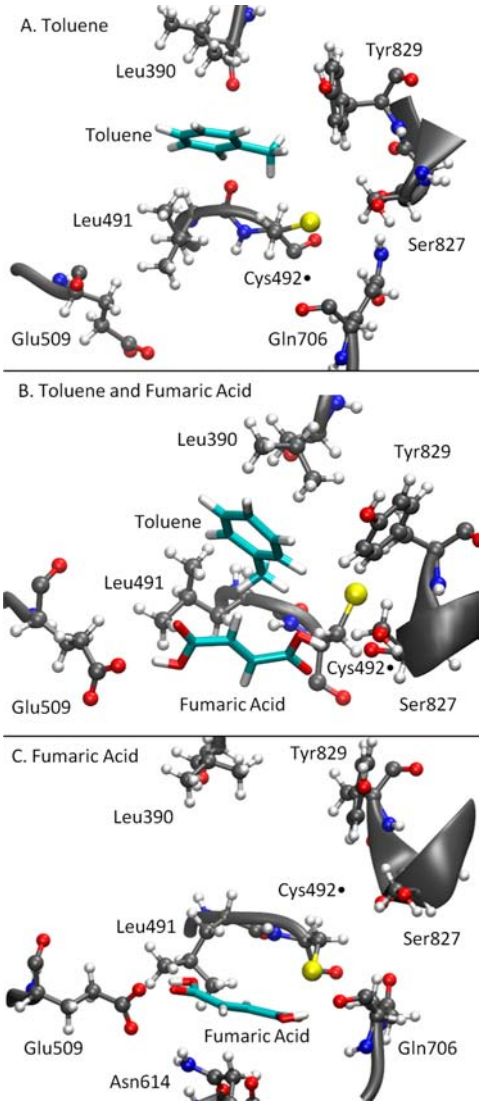

Figure 5. Enzyme–substrate interactions at the active site observed during MD simulations of (A) toluene alone, (B) toluene and fumaric acid, and (C) fumaric acid alone at the active site. The substrates are shown in licorice representation with the carbon atoms colored cyan. The protein backbone and the residues close to the ligand are indicated with ribbon and CPK representations, respectively.

succinate product binding is aided by both the hydrophobic and polar active site residues (Supporting Information Figure 8).

Although it has been experimentally observed that the *R*-stereoisomer of benzylsuccinate is predominantly formed, there appears to be no distinction between the two isomers in their binding characteristics and dynamics at the active site. As observed in other enzyme systems, the preference for a specific stereoisomer could occur through either racemization or inversion.[69,70] Racemization would involve a configurational change in the intermediate benzylsuccinyl radical that determines the stereochemistry of the final product. This would require sufficient residence time for the succinyl radical intermediate and could possibly be aided by an allosteric modification at the active site. On the other hand, if the stereochemical preference is determined via inversion, the stereochemistry would indicate a concerted reaction mechanism which would involve the orientation of the cysteine radical, methyl group of toluene, and fumaric acid to directly result in the formation of *R*-benzylsuccinate. It has been demonstrated, based on recent studies on alkylsuccinate synthase, a recently discovered fumarate addition enzyme closely related to BSS, that the stereospecific nature of the product is determined due to inversion.[70] The orientation of the substrates observed in this study ensures the geometric feasibility for an inversion mechanism; however, since the stereoisomers are a result of a distinct reaction mode, determining the exact mechanism responsible for BSS's stereochemical preference for the *R*-isomer necessitates a more detailed study of the plausible reaction schemes, utilizing higher level ab initio or hybrid QM/MM methods which are beyond the scope of this study and are the subject of further studies on this enzyme.

3.4. Alanine Mutants Reveal the Impact of Specific Residues on Substrate Binding. The geometric and energetic analyses outlined above point to the involvement of Phe384, Leu390, Leu491, Tyr829, and Val708 in stabilizing toluene binding and Ser827, Glu509, and Gln706 in stabilizing fumaric acid binding. Systematic point mutations of these residues to alanine help assess and quantify their role in enabling substrate binding. Table 2 lists the energetic impact of these mutations on toluene and fumaric acid binding. Positive values indicate that the mutation impacts substrate binding unfavorably and can be considered as prime candidates for performing experimental point mutational analysis.

Table 2. Impact of Alanine Mutations on Toluene and Fumaric Acid Binding Energies

Mutation	$\Delta\Delta G_{binding} = \Delta G_{mutant} - \Delta G_{wild\ type}$
Effect on Toluene Binding	
Phe384Ala	1.9 ± 0.9 kcal/mol
Leu491Ala	1.2 ± 0.7 kcal/mol
Leu390Ala	2.0 ± 0.8 kcal/mol
Val708Ala	1.1 ± 0.6 kcal/mol
Tyr829Ala	1.8 ± 0.7 kcal/mol
Effect on Fumaric Acid Binding	
Glu509Ala	5.4 ± 1.9 kcal/mol
Gln706Ala	3.9 ± 1.9 kcal/mol
Ser827Ala	5.7 ± 1.8 kcal/mol

The alanine scanning mutations clearly indicate that the mutations of Leu390 and Phe384 have the greatest impact on toluene binding with binding energies shifting unfavorably by ~2 kcal/mol in both cases. The most significant impacts on fumaric acid binding were affected by the Glu509Ala and Ser827Ala mutations with an impact of 5.4 and 5.7 kcal/mol, respectively. The larger perturbation seen for fumaric acid binding is due to the stronger character of the hydrogen bonding network as opposed to $\pi-\pi$ and hydrophobic interactions that stabilize toluene. To compensate for the smaller magnitude interactions with toluene it is found that more hydrophobic interactions are recruited to stabilize its binding.

3.5. Geometric Implications for the Catalytic Mechanism. The glycyl/thiyl Cα (GlyCα–CysCα) distances and glycyl Cα/thiyl sulfur (GlyCα–CysS) distances have been described as characteristics specific to GREs. The average values of these (GlyCα–CysCα and GlyCα–CysS) distances observed in the seven BSSα systems prepared in this study (Table 3) are consistent with other structurally characterized GREs (Supporting Information Table 7). The averages and

dx.doi.org/10.1021/ja404842r | J. Am. Chem. Soc. 2013, 135, 12279–12288

Table 3. Average Distances, Standard Deviations, and Percentage of Simulation Time When Feasible H-Transfer Distances Were Observed over the 40 ns MD Trajectories of Each of the Systems

	Gly828Cα−Cys492•Cα	Gly828Cα−Cys492•S		Cys492•S−toluene/benzylsuccinate	
System	average (Å)	average (Å)	productive[a]	average (Å)	productive[a]
BSSα (nonradical form)	4.9 ± 0.5	4.0 ± 0.3	-	-	-
BSSα	6.1 ± 0.7	5.9 ± 0.6	0.0%	-	-
BSSα + fumaric acid	5.5 ± 0.5	6.7 ± 1.2	10.5%	-	-
BSSα + toluene	6.2 ± 0.8	5.6 ± 1.1	15.3%	6.7 ± 1.5	10.8%
BSSα + toluene + fumaric acid	5.9 ± 0.9	4.7 ± 1.1	51.4%	5.3 ± 0.7	5.8%
BSSα + *R*-succinate	6.4 ± 0.5	4.1 ± 0.4	88.1%	4.5 ± 0.8	57.6%
BSSα + *S*-Succinate	5.6 ± 0.3	3.9 ± 0.3	97.3%	5.1 ± 1.0	39.7%

[a]Productive (%) indicates the percentage of the simulation time when the distance between the atoms was less than 4.5 Å.

standard deviations have been calculated based on the 40 ns simulations for each system. The standard deviation values for these distances can be seen as an indication of the fluctuations in the system. The significantly lower standard deviations observed for all distances in the case with both substrates bound (BSSα + Toluene + Fumaric Acid) is indicative of substrate binding stabilizing the active site. This suggests that the presence of both substrates at the active site is necessary for the reaction and reaffirms the proposed reaction mechanism. Martins et al. observed a reduction in the Gly−Cys distance in HPA-D by 0.4 Å upon substrate binding.[62] The average GlyCα−CysCα distance in BSSα is also observed to decrease by 0.3 Å upon fumaric acid and toluene binding (Table 3, Row 2−Row 5). This also corroborates observations that substrate binding results in a more compact active site.[62] The average values also reproduce the trends observed in experimental structures where the GlyCα−CysS distance is, in most cases, shorter than the GlyCα−CysCα distance (Supporting Information Table 7).

It is also known that H-transfer distances in other radical enzymes (biotin synthase, PFL activating enzymes, etc.) are in the range of 3.5−4.1 Å.[62] Given the plausible radical transfer pathway governing fumarate addition in BSS (Scheme 1), we would expect distances between molecules involved in radical transfer for BSS to be in the same range.[11] The MD simulations in this study provide an opportunity to evaluate the feasibility of the proposed mechanism for fumarate addition in BSSα. The possible radical transfer distances in BSSα, namely, (i) Gly828Cα−Cys492•S and (ii) Cys492•S−Toluene (methyl carbon) or Cys492•S−benzylsuccinate (central carbon), were evaluated from the MD simulations of the seven different systems in this study. On the basis of the H-transfer distances observed in radical enzymes and the Cα−S distances observed in GRE crystal structures, a cutoff distance of 4.5 Å for feasible H-transfer distance was considered. Conformations during the simulation meeting this cutoff were considered to be productive (Table 3). In the MD simulations of toluene alone and with fumaric acid, it was observed that the methyl group of toluene pivots about its ring position resulting in higher average distances and lower percentage of productive radical transfer distances. This is due to the reduced interactions with Val708 and higher interactions with Leu390 in the absence of fumaric acid. In the presence of fumaric acid the interactions with Val708 dramatically increase, significantly stabilizing toluene. In the case of benzylsuccinate, the lower average distances are attributed to its decreased flexibility compared to the reactants and stable hydrogen bonding with Ser827, Gln706, and Val 708. *Most importantly, all systems consistently demonstrate conformations for feasible H-transfer, indicating a feasible structural basis from which to initiate further studies on the* reaction *mechanism.*

Although the active site glycine is known to harbor the radical (glycyl radical) and is believed to be more stable, the thiyl radical is suggested to mediate the reaction.[17,71] This is plausible considering its proximal location to both substrates and its inherent orientational flexibility, enabling the radical transfer reactions involved in the mechanism. To clearly identify the impact of substrate and product binding on the flexibility of the active site cysteine, and therefore the reaction mechanism, the potential of mean force (PMF) for the dihedral rotation of the thiyl radical was evaluated. In the absence of substrates, the PMF depicts two thermodynamically equivalent wells at −60° and +60° that are separated by an energy barrier of 5.7 kcal/mol at 0° (Figure 6). However, upon substrate binding, the well around +60° is made thermodynamically

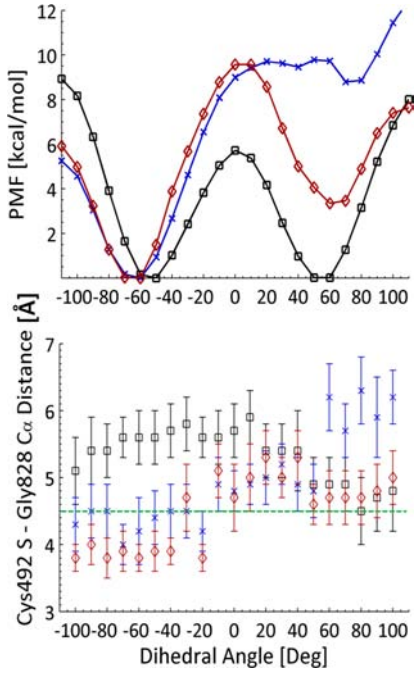

Figure 6. (Top) PMFs for the N−C_α−C_β−S dihedral rotation in the presence of substrates (×, blue), without substrates (□, black) and in the presence of product (◊, dark red). (Bottom) The errors in the PMFs are <0.1 kcal/mol as determined by bootstrap analysis. Average cysteine−glycine radical transfer distance as observed along the dihedral angle for the three systems. The dashed line demarcates the cutoff distance (4.5 Å) for the productive radical transfer distances assumed in this study.

dx.doi.org/10.1021/ja404842r | J. Am. Chem. Soc. 2013, 135, 12279−12288

unfavorable by 9.5 kcal/mol and is separated by an increased barrier of 9.7 kcal/mol. The presence of the product is characterized by the same increased barrier as seen with the substrate-bound case; however, the second well appears to be more stable as compared to the substrate-bound case and less stable than the unbound case. Thus, substrate/product binding restricts the orientational flexibility of the thiyl radical to a well-described region between −70° and −40° for the N−Cα−C$_\beta$−S torsion.

An analysis of the average CysS−GlyCα distances observed during the 2 ns simulations at each window along the rotation of the dihedral (Figure 6) reveals the impact of this restriction on possible radical transfer pathways. The lowest average radical transfer distances are found when substrate/product is bound and occur in the thermodynamically stable well (−70° to −40°) observed in the PMFs. This is in agreement with experimental observations in the case of HPA-D, where Martins et al. hypothesized that substrate binding could lead to conformational rearrangement of the active site to generate the thiyl radical and initiate the reaction mechanism.[62] An analysis of the productive instances (<4.5 Å) for CysS-toluene/benzylsuccinate radical transfer distances also indicates that the productive well (−70° to −40°) is more conducive for radical transfer.

These observations suggest that substrate binding restricts the conformation of the cysteine residue to increase the feasibility for radical transfer. The radical transfer pathway scheme involved in the fumarate addition mechanism is likely to be substrate assisted and supports the proposed reaction mechanism (Scheme 1).

4. CONCLUSIONS

A combined computational approach involving homology modeling, docking, MD simulations, MM/GBSA binding energy calculations, alanine scanning, and umbrella sampling methods have been employed to elucidate the active site topology and the substrate dynamics in BSSα. Furthermore, enzyme−substrate interactions in an active radical enzyme system have been explored using MD simulations. The successful application of the parameterized cysteine radical in this study bodes well for its application to investigate other enzyme systems that involve cysteine radicals. Putative binding pockets for the substrates toluene and fumaric acid have been identified and are found to be conserved in BSSα from various bacterial species.

The predicted active site topology of BSSα is suggested to consist of a hydrophobic pocket (Phe384, Leu390, Leu491, Val708, and Tyr829) conducive for toluene binding and a polar region (Glu509, Ser827, and Gln706) favoring fumaric acid binding. The MM/GBSA binding energies demonstrate that the active site topology is able to bind both substrates favorably. Alanine scanning experiments reveal that Phe384, Leu390, Glu509, and Gln706 are particularly important in ensuring the binding of substrates. The hydrogen bonding network aided by Glu509, Ser827, and Gln706 is found to be crucial in stabilizing fumaric acid and enabling toluene addition.

In the context of the fumarate addition reaction mechanism, MD simulations of BSSα in the presence of substrates suggests the plausibility of the proposed mechanism by demonstrating (i) the *syn* addition of toluene to fumaric acid and (ii) facilitating a mechanism that retains the hydrogen abstracted from the methyl group of toluene within the succinyl moiety. It has also been demonstrated that substrate binding impacts dynamics at the active site to favor feasible radical transfer pathways as demonstrated by a tighter active site and the restricted mobility of the thiyl radical. The structural basis for the fumarate addition reaction in BSSα, elucidated in this study, provides a link between interpreting available experimental data and designing future studies, both theoretical and experimental in nature, to further our limited understanding of the remarkable free radical mechanism(s) employed by BSSα.

■ ASSOCIATED CONTENT

Supporting Information

Multiple sequence alignments for homology modeling, validation of the homology modeling coupled with docking approach, parameterization procedure for the CYR amino acid residue, optimized geometries and energies for the model systems used for RESP calculations, detailed BLAST results, Verify3D analysis of the homology model, results of the independent substrate docking studies for toluene and fumaric acid, RMSD and RMSF analyses of the homology model from MD simulations, MM/GBSA and decomposition analysis, details of the geometric and hydrogen bond analysis for toluene, fumaric acid, and benzylsuccinate, and comparison of the glycyl/thiyl Cα (GlyCα−CysCα) distances and glycyl Cα/thiyl sulfur (GlyCα−CysS) distances for GREs. This material is available free of charge via the Internet at http://pubs.acs.org.

■ AUTHOR INFORMATION

Corresponding Author

cmmaupin@mines.edu

Notes

The authors declare no competing financial interest.

■ ACKNOWLEDGMENTS

Funding provided by ONR MURI Grant N00014-10-1-0946. The authors would like to acknowledge financial support from Dr. David Shifler at the Office of Naval Research, under Award N00014-10-1-0946, the Golden Energy Computing Organization at the Colorado School of Mines for the use of computational resources, and thank Dr. Shubham Vyas and Dr. Venkata Somisetti for their helpful discussions during the preparation of the manuscript.

■ REFERENCES

(1) Frey, P. A. *Annu. Rev. Biochem.* **2001**, *70*, 121.
(2) Selmer, T.; Pierik, A. J.; Heider, J. *Biol. Chem.* **2005**, *386*, 981.
(3) Eklund, H.; Fontecave, M. *Structure* **1999**, *7*, R257.
(4) Widdel, F.; Rabus, R. *Curr. Opin. Biotechnol.* **2001**, *12*, 259.
(5) Foght, J. *J. Mol. Microb. Biotechnol.* **2008**, *15*, 93.
(6) Heider, J.; Spormann, A. M.; Beller, H. R.; Widdel, F. *FEMS Microbiol. Rev.* **1998**, *22*, 459.
(7) Duncan, K. E.; Gieg, L. M.; Parisi, V. A.; Tanner, R. S.; Tringe, S. G.; Bristow, J.; Suflita, J. M. *Environ. Sci. Technol.* **2009**, *43*, 7977.
(8) Aktas, D. F.; Lee, J. S.; Little, B. J.; Ray, R. I.; Davidova, I. A.; Lyles, C. N.; Suflita, J. M. *Energy Fuels* **2010**, *24*, 2924.
(9) Dean, B. J. *Mutat. Res.-Rev. Genet.* **1985**, *154*, 153.
(10) Li, L.; Patterson, D. P.; Fox, C. C.; Lin, B.; Coschigano, P. W.; Marsh, E. N. G. *Biochemistry* **2009**, *48*, 1284.
(11) Krieger, C. J.; Roseboom, W.; Albracht, S. P. J.; Spormann, A. M. *J. Biol. Chem.* **2001**, *276*, 12924.
(12) Qiao, C. H.; Marsh, E. N. G. *J. Am. Chem. Soc.* **2005**, *127*, 8608.
(13) Li, L.; Marsh, E. N. G. *Abstr. Pap. Am. Chem. Soc.* **2009**, *237*, 397.
(14) Li, L.; Marsh, E. N. G. *J. Am. Chem. Soc.* **2006**, *128*, 16056.
(15) Li, L.; Marsh, E. N. G. *Biochemistry* **2006**, *45*, 13932.

(16) Reddy, S. G.; Wong, K. K.; Parast, C. V.; Peisach, J.; Magliozzo, R. S.; Kozarich, J. W. *Biochemistry* **1998**, *37*, 558.
(17) Himo, F. *J. Phys. Chem. B* **2002**, *106*, 7688.
(18) Fan, H.; Hitchcock, D. S.; Seidel, R. D.; Hillerich, B.; Lin, H.; Almo, S. C.; Sali, A.; Shoichet, B. K.; Raushel, F. M. *J. Am. Chem. Soc.* **2012**, *135*, 795.
(19) Mitcheson, J. S.; Chen, J.; Lin, M.; Culberson, C.; Sanguinetti, M. C. *Proc. Natl. Acad. Sci. U.S.A.* **2000**, *97*, 12329.
(20) Essigmann, B.; Hespenheide, B. M.; Kuhn, L. A.; Benning, C. *Arch. Biochem. Biophys.* **1999**, *369*, 30.
(21) Genheden, S. *J. Chem. Inf. Model.* **2012**, *52*, 3013.
(22) Harel, M.; Sussman, J. L.; Krejci, E.; Bon, S.; Chanal, P.; Massoulié, J.; Silman, I. *Proc. Natl. Acad. Sci.* **1992**, *89*, 10827.
(23) Huang, X. Q.; Zheng, F.; Zhan, C. G. *J. Am. Chem. Soc.* **2008**, *130*, 16691.
(24) Cole, D. I.; Legassie, J. D.; Bonifacio, L. N.; Sekaran, V. G.; Ding, F.; Dokholyan, N. V.; Jarstfer, M. B. *J. Am. Chem. Soc.* **2012**, *134*, 20070.
(25) Beller, H. R.; Spormann, A. M. *J. Bacteriol.* **1998**, *180*, 5454.
(26) Shinoda, Y.; Sakai, Y.; Uenishi, H.; Uchihashi, Y.; Hiraishi, A.; Yukawa, H.; Yurimoto, H.; Kato, N. *Appl. Environ. Microb.* **2004**, *70*, 1385.
(27) Johnson, M.; Zaretskaya, I.; Raytselis, Y.; Merezhuk, Y.; McGinnis, S.; Madden, T. L. *Nucleic Acids Res.* **2008**, *36*, W5.
(28) O'Brien, J. R.; Raynaud, C.; Croux, C.; Girbal, L.; Soucaille, P.; Lanzilotta, W. N. *Biochemistry* **2004**, *43*, 4635.
(29) Lehtiö, L.; Günter Grossmann, J.; Kokona, B.; Fairman, R.; Goldman, A. *J. Mol. Biol.* **2006**, *357*, 221.
(30) Becker, A.; Fritz-Wolf, K.; Kabsch, W.; Knappe, J.; Schultz, S.; Wagner, A. F. V. *Nat. Struct. Biol.* **1999**, *6*, 969.
(31) Marti-Renom, M. A.; Stuart, A. C.; Fiser, A.; Sanchez, R.; Melo, F.; Sali, A. *Annu. Rev. Biophys. Biomol.* **2000**, *29*, 291.
(32) Marti-Renom, M. A.; Madhusudhan, M. S.; Sali, A. *Protein Sci.* **2004**, *13*, 1071.
(33) Melo, F.; Sali, A. *Protein Sci.* **2007**, *16*, 2412.
(34) Shen, M. Y.; Sali, A. *Protein Sci.* **2006**, *15*, 2507.
(35) Pettersen, E. F.; Goddard, T. D.; Huang, C. C.; Couch, G. S.; Greenblatt, D. M.; Meng, E. C.; Ferrin, T. E. *J. Comput. Chem.* **2004**, *25*, 1605.
(36) Eisenberg, D.; Luthy, R.; Bowie, J. U. *Methods Enzymol.* **1997**, *277*, 396.
(37) Laskowski, R. A.; Macarthur, M. W.; Moss, D. S.; Thornton, J. M. *J. Appl. Crystallogr.* **1993**, *26*, 283.
(38) Hetenyi, C.; van der Spoel, D. *Protein Sci.* **2002**, *11*, 1729.
(39) Reeves, D. C.; Sayed, M. R. F.; Chau, P. L.; Price, K. L.; Lummis, S. C. R. *Biophys. J.* **2003**, *84*, 2338.
(40) de Graaf, C.; Vermeulen, N. P. E.; Feenstra, K. A. *J. Med. Chem.* **2005**, *48*, 2725.
(41) Morris, G. M.; Huey, R.; Lindstrom, W.; Sanner, M. F.; Belew, R. K.; Goodsell, D. S.; Olson, A. J. *J. Comput. Chem.* **2009**, *30*, 2785.
(42) Hornak, V.; Abel, R.; Okur, A.; Strockbine, B.; Roitberg, A.; Simmerling, C. *Proteins* **2006**, *65*, 712.
(43) Case, D. A.; Darden, T. A.; Cheatham, T.E., III; Simmerling, C.L.; Wang, J.; Duke, R. E.; Luo, R.; Walker, R.C.; Zhang, W.; Merz, K. M.; Roberts, B.; Hayik, S.; Roitberg, A.; Seabra, G.; Swails, J.; Goetz, A. W.; Kolossváry, I.; Wong, K. F.; Paesani, F.; Vanicek, J.; Wolf, R. M.; Liu, J.; Wu, X.; Brozell, S. R.; Steinbrecher, T.; Gohlke, H.; Cai, Q.; Ye, X.; Wang, J.; Hsieh, M.-J.; Cui, G.; Roe, D. R.; Mathews, D. H.; Seetin, M. G.; Salomon-Ferrer, R.; Sagui, C.; Babin, V.; Luchko, T.; Gusarov, S.; Kovalenko, A.; Kollman, P. A. *Amber12 and AmberTools12*; University of California: San Fransisco, 2012.
(44) Wang, J. M.; Wolf, R. M.; Caldwell, J. W.; Kollman, P. A.; Case, D. A. *J. Comput. Chem.* **2004**, *25*, 1157.
(45) Anandakrishnan, R.; Aguilar, B.; Onufriev, A. V. *Nucleic Acids Res.* **2012**, *40*, W537.
(46) Jorgensen, W. L.; Chandrasekhar, J.; Madura, J. D.; Impey, R. W.; Klein, M. L. *J. Chem. Phys.* **1983**, *79*, 926.
(47) Ryckaert, J.-P.; Ciccotti, G.; Berendsen, H. *J. Comput. Phys.* **1977**, *23*, 327.
(48) Humphrey, W.; Dalke, A.; Schulten, K. *J. Mol. Graphics Modell.* **1996**, *14*, 33.
(49) Miller, B. R.; McGee, T. D.; Swails, J. M.; Homeyer, N.; Gohlke, H.; Roitberg, A. E. *J. Chem. Theory Comput.* **2012**, *8*, 3314.
(50) Kollman, P. A.; Massova, I.; Reyes, C.; Kuhn, B.; Huo, S. H.; Chong, L.; Lee, M.; Lee, T.; Duan, Y.; Wang, W.; Donini, O.; Cieplak, P.; Srinivasan, J.; Case, D. A.; Cheatham, T. E. *Acc. Chem. Res.* **2000**, *33*, 889.
(51) Li, L.; Li, Y. Y.; Zhang, L. L.; Hou, T. J. *J. Chem. Inf. Model.* **2012**, *52*, 2715.
(52) Xue, W. W.; Liu, H. X.; Yao, X. J. *J. Comput. Chem.* **2012**, *33*, 527.
(53) Zoete, V.; Meuwly, M.; Karplus, M. *Proteins* **2005**, *61*, 79.
(54) Sabbah, D. A.; Vennerstrom, J. L.; Zhong, H. Z. A. *J. Chem. Inf. Model.* **2012**, *52*, 3213.
(55) Zhong, H. Z.; Carlson, H. A. *Proteins* **2005**, *58*, 222.
(56) Cao, R. Y.; Jin, Y. D.; Xu, D. G. *J. Phys. Chem. B* **2012**, *116*, 6087.
(57) Li, M. H.; Zheng, W. J. *Biochemistry* **2011**, *50*, 8645.
(58) Zoete, V.; Michielin, O. *Proteins* **2007**, *67*, 1026.
(59) Shankar, K.; Djamal, B.; Robert, H. S.; Peter, A. K.; John, M. R. *J. Comput. Chem.* **1992**, *13*, 1011.
(60) Roux, B. *Comput. Phys. Commun.* **1995**, *91*, 275.
(61) Grossfield, A.; *WHAM*, 2.0.6 ed.; http://membrane.urmc.rochester.edu/content/wham.
(62) Martins, B. M.; Blaser, M.; Feliks, M.; Ullmann, G. M.; Buckel, W.; Selmer, T. *J. Am. Chem. Soc.* **2011**, *133*, 14666.
(63) Wöhlbrand, L.; Jacob, J. H.; Kube, M.; Mussmann, M.; Jarling, R.; Beck, A.; Amann, R.; Wilkes, H.; Reinhardt, R.; Rabus, R. *Environ. Microbiol.* **2012**, 1334.
(64) Leuthner, B.; Leutwein, C.; Schulz, H.; Horth, P.; Haehnel, W.; Schiltz, E.; Schagger, H.; Heider. *J. Mol. Microbiol.* **1998**, *28*, 615.
(65) Kühner, S.; Wöhlbrand, L.; Fritz, I.; Wruck, W.; Hultschig, C.; Hufnagel, P.; Kube, M.; Reinhardt, R.; Rabus, R. *J. Bacteriol.* **2005**, *187*, 1493.
(66) Achong, G. R.; Rodriguez, A. M.; Spormann, A. M. *J. Bacteriol.* **2001**, *183*, 6763.
(67) Larkin, M. A.; Blackshields, G.; Brown, N. P.; Chenna, R.; McGettigan, P. A.; McWilliam, H.; Valentin, F.; Wallace, I. M.; Wilm, A.; Lopez, R.; Thompson, J. D.; Gibson, T. J.; Higgins, D. G. *Bioinformatics* **2007**, *23*, 2947.
(68) Paul, B.; Das, D.; Ellington, B.; Marsh, E. N. G. *J. Am. Chem. Soc.* **2013**, *135*, 5234.
(69) Ahn, Y.; Ye, Q.; Cho, H.; Walsh, C. T.; Floss, H. G. *J. Am. Chem. Soc.* **1992**, *114*, 7953.
(70) Jarling, R.; Sadeghi, M.; Drozdowska, M.; Lahme, S.; Buckel, W.; Rabus, R.; Widdel, F.; Golding, B. T.; Wilkes, H. *Angew. Chem., Int. Ed.* **2012**, *51*, 1334.
(71) Himo, F. *Chem. Phys. Lett.* **2000**, *328*, 270.